Supporting Information

Jianye Fu,[a] Zhengying Gu,[a] Yang Liu,[a] Jun Zhang,[a] Hao Song,[a] Yannan Yang,[a] Yang Yang,[a] Owen Noonan,[a] Jie Tang,[a] and Chengzhong Yu*[a][b]*

[a] J. Fu, Z. Gu, Dr. Y. Liu, Dr. J. Zhang, Dr. H. Song, Dr. Y. Yang, Y. Yang, Dr. O. Noonan, Dr. J. Tang* and Prof. C. Yu*
Australian Institute for Bioengineering and Nanotechnology, the University of Queensland, St Lucia, Brisbane, QLD 4072, Australia
E-mail: j.tang3@uq.edu.au; c.yu@uq.edu.au

[b] Prof. C. Yu*
School of Chemistry and Molecular Engineering East China Normal University Shanghai 200241, P. R. China
E-mail: czyu@chem.ecnu.edu.cn

Cell culture

Cell culture reagents were all purchased from GIBCO Invitrogen Corporation/Life Technologies Life Sciences. All cell lines were purchased from ATCC (CellBank Australia). CHO-K1 cells were cultured in Dulbecco's Modified Eagle Medium (DMEM): Nutrient Mixture F-12 (DMEM/F-12) supplemented with 10% fetal bovine serum (FBS) and 1% penicillin-streptomycin (PS). RAW264.7, HCT116 and KHOS cell lines were cultured in DMEM supplemented with 10% FBS and 1% PS. HCT116, CHO-K1 and KHOS cells were cultured in T75 flasks while RAW264.7 cells were cultured in petri dish. All cells were cultured at 37 ^{o}C with 5% CO_2.

Cellular uptake evaluated by ICP-OES

The cellular uptake was quantitatively studied between the J-SNPs and S-SNPs. 2×10^5 cells/well of each cell lines were seeded in 6-well plates for 24 h before the uptake experiment. The J-SNPs or S-SNPs (100 μg/well, with concentration of 50 μg/mL) were incubated with cells at 0.5, 2 and 4 h. Afterwards, the cells were trypsinized and collected, followed by being washed with phosphate buffered saline (PBS) and transferred to 2 mL microcentrifuge tubes (If it is macrophage, 1 mL warm PBS was used to gently wash off particles attached on cells, then 1 mL cold PBS was used to make cells detached from the dishes). Cell counting was performed by a hemocytometer after cell collection. Then cells were centrifuged again and the supernatant was removed. 120 μL cell lysis buffer was added to allow the cells to break apart in ultrasonic water bath. The pellets were collected by centrifugation at 13,000 rpm for 10 min. Aqueous NaOH solution (1 M) was then added to dissolve the pellets for 24 h. The silicon content in the final solutions were measured by ICP-OES, the result of which were then converted into silica amount.

Confocal fluorescence microscopy assays for actin staining

Each cell line was cultured on a sterile coverslip in a 6-well plate with a density of 2×10^5 cells per well. After culturing for 24 h, the J-SNPs or S-SNPs (100 μg/well, with concentration of 50 μg/mL) were further incubated with cells for 0.5, 2 and 4 h. At each time point, cell culture medium was removed, 1 mL warm PBS was used to gently wash off attached particles for twice. The cells were fixed with 4% electron microscopy-grade paraformaldehyde (PFA) for 30 min. Once fixed, the cells were washed with PBS and permeabilized with 0.1% Triton X-100 in PBS for 3 min. Then the cells were washed again with PBS and 2.5 units/mL rhodamine phalloidin was added to each well for 15 min to stain polymerized actin filaments. Each well was washed with PBS. The coverslips were taken out, stuck on glass slides and viewed at 63× magnification. Bright-field and fluorescent images of cells were acquired and merged. The phagocytosis level was determined by the obtained red fluorescence intensity. To visually detect the fluorescent intensity coming from the activation of phagocytosis, the confocal microscopy parameters were set to offset the fluorescent signals from the control group (PBS treated sample) of each cell line.

Grafting of rhodamine-B-isothiocyanate (RITC) on silica nanoparticles

3 mg of RITC was reacted with 20 μL (3-aminopropyl)triethoxysilane (APTES) in 1 mL ethanol solution under dark condition for 24 h. Subsequently, 4 mg of the silica nanoparticles were reacted with the as prepared 1 mL RITC-APTES stock solution under dark conditions for 24 h. The RITC grafted silica nanoparticles were collected by centrifugation and washed with ethanol several times to remove the free dye molecules. To normalize the RITC amount in each type of silica nanoparticles, ~1 mg RITC grafted silica nanoparticles were dissolved in NaOH solution aqueous (1 M). The RITC concentrations were then measured by UV-Vis spectroscopy. The RITC grafting density was measured to be 4.6 μg/mg and 5.3 μg/mg for J-SNPs and S-SNPs, respectively.

Cellular uptake of nanoparticles evaluated by confocal fluorescence microscopy

Each cell line was cultured on a sterile coverslip in a 6-well plate with a density of 2×10^5 cells per well. After culturing for 24 h, the RITC conjugated J-SNPs or S-SNPs (100 μg/well) were further incubated with cells for 4 h. The cells were fixed and the cell nuclei were stained by DAPI (blue fluorescence). The samples were observed under a fluorescence microscope (Leica SP8).

MTT assay

The potential biotoxicity of J-SNPs or S-SNPs were tested in RAW264.7, HCT116, CHO-K1 and KHOS cell lines. 8000 cells were seeded in each well of 96-well plates. After incubation for 24 h, the medium was replaced with 100 uL fresh medium. Then 100 uL of particle medium solution with different particle concentration were prepared and added to each well. After further incubation for 24 h and 72 h, 20 uL MTT PBS solution (5 mg/mL) were added to each well. Incubation for 4 h, then the culture medium was replaced with 200 uL dimethyl sulfoxide (DMSO). The related absorbance were recorded at 540 nm using a Tecan Infinite M200 PRO microplate reader.

Fluorescence-activated cell sorting (FACS) analysis of cytochalasin D (noted as Cyto D) inhibited cellular uptake in RAW264.7 cell line

The density of 1×10^5 cell/well and 12-well plates were used for seeding. The cell culture and sample preparation was the same with cellular uptake except without cell lysis. Before the incubation of SNPs with cells, Cyto D (10 μg/well) was introduced in the culture medium and incubated for 0.5 h at 37 ^{o}C. Afterwards, RITC conjugated J-SNPs and S-SNPs (50 μg/well) was added to the culture medium and incubated for another 0.5 h. Cells were collected and analysed by CytoFLEX flow cytometer. The results were reported as the mean fluorescence

intensity obtained by measuring 10,000 cells between independent experiments. Error bars represent one standard deviation around the mean.

Scanning electron microscopy (SEM) observation of J-SNPs on cells

Cells were grown on Thermonox coverslips (Nunc, Roskilde, Denmark) and treated with particles for 1 h. After incubation, the medium was removed and the samples were gentle washed by PBS. The cell samples were then fixed by 50 μl formalin (10%) for 1 h. After washed by PBS, the cells were stained by 50 μl osmium tetroxide for 2 h. The cell samples were then dehydrated in increasing concentrations of ethanol solution (50, 60, 70, 80, 90, 95 and 100%) for 5 min each. Then the sample were mounted and gold sputter coated before examination SEM.

Synthesis of MCM-48

MCM-48 mesoporous silica nanoparticles were synthesized according to a literature report.[1] In a typical synthesis, 500 mg of cetyltrimethylammonium bromide (CTAB) and 1 g of F127 were dissolved in an aqueous solution containing 96 mL distilled water, 10 g of ammonium hydroxide solution (28 wt%) and 34 g of ethanol. Afterwards, 1.8 g of TEOS was added into the above solution and vigorously stirred for 1 min. Then the mixture was kept under static solution for 24 h at room temperature.

Synthesis of dendritic mesoporous organosilica nanoparticles (DMSNs)

Dendritic mesoporous organosilica nanoparticles (DMSNs) were synthesized according to literature with slight modification.[2] At first, 380 mg of CTAB and 168 mg of sodium salicylate were added in 25 mL of water containing 68 mg of triethanolamine (TEA). Afterwards, 6 mL of TEOS was added to the above solution and vigorously stirred for 4 h under 80 °C.

In vitro human intestine Caco-2/M cell model and nanoparticles transportation across Caco-2/M cell monolayer

An in vitro human intestine Caco-2/M cell model was cultured to investigate the transcellular uptake of J-SNPs and S-SNPs. The human intestine Caco-2/M cell model was obtained based on previous reported protocols.[3,4] Briefly, 500 μL culture medium containing 5×10^5 Caco-2 cells were seeded on the apical side of a polyethylene terephthalate (PET) transwell filter inserted in a 12-well plate. Then 1.5 ml medium was added to the basolateral sides. The culture medium was changed every other day and the cells were allow growth for 14 days. Then, 5×10^5 Raji B cells suspended in RPMI-1640 culture medium were added to the basolateral compartment of the inserts to trigger M cell differentiation. The Caco-2/M cell coculture monolayer was maintained for 7 days and the medium in the apical side of the transwell was changed every other day.

In the nanoparticles transportation across Caco-2/M cell monolayer experiment, the cells were washed twice with PBS and pre-equilibrated for 1 h with Hanks' balanced salt solution (HBSS) buffered at pH 7.4 prior to the transportation experiment. Afterwards, J-SNPs or S-SNPs (labelled by RITC, 50 ug/mL in HBSS pH 7.4) were added on the apical side of the monolayers and incubated for 0.5, 2 or 4 h. Samples (200 μL) were taken from the basolateral side and the amount of J-SNPs and S-SNPs transported through the Caco-2/M cell monolayer was determined using a fluorescence 96-wells plate reader. The excitation and emission wavelengths used were 570 and 595 nm, respectively. In the experiment of evaluating the uptake and transported amount of FITC-OVA loaded nanoparticles, the excitation and emission wavelengths used were 490 and 525 nm, respectively.

Additionally, to visualize the uptake and transport of J-SNPs and S-SNPs by M cells or other enterocytes in the Caco-2/M-cell monolayer, we performed Alexa Fluor 488 fluorescence labelled wheat germ agglutinin (WGA)/Hoechst 33342 double staining to monitor glycosidic

moieties that differentially expressed by M cells.[5] Briefly, M cells were co-stained with 0.5 mL of WGA Alexa Fluor 488/Hoechst 33342 and were incubated for 10 min at 37 ^{o}C/5% CO_2 in the dark. Afterward, cells were washed two times with HBSS and fixed before samples were observed using fluorescence microscopy (Leica SP8).

Characterizations:

Transmission electron microscopy (TEM) measurements were obtained on a HT7700 (Hitachi) microscope. Scanning electron microscopy (SEM) images were taken by a JEOL JSM-7800F Field Emission Electron Microscope operated at 0.5 KV. The electron tomography (ET) specimens were prepared by dispersing nanoparticles in ethanol and then deposition of the suspension onto copper grids. The tomographic tilt series were carried out by tilting the specimen inside the microscope around at an increment of 1^{o} under the electron beam. Micromeritics Tristar 3000 system was carried out for Nitrogen adsorption/desorption experiments at -196 ^{o}C. The samples were pre-treated under vacuum line at 150 ^{o}C overnight. The Brunauer-Emmett-Teller (BET) method was utilized to calculate the specific surface areas by using the adsorption data at a relative pressure (P/P_0) range of 0.05-0.35. Barrett-Joyner-Halanda (BJH) method was utilized to obtain the pore-size distribution curves of the samples from the adsorption branch of the isotherms and the total pore volume. The total pore volume was calculated from the amount adsorbed at a maximum P/P_0 of 0.99. Dynamic light scattering (DLS) were carried out at 25 ^{o}C using a Zetasizer Nano-ZS from Malvern Instruments. To determine the stability of nanoparticle dispersions, the DLS profiles of J-SNPs and S-SNPs dispersed in PBS solutions were monitored for 24 h.

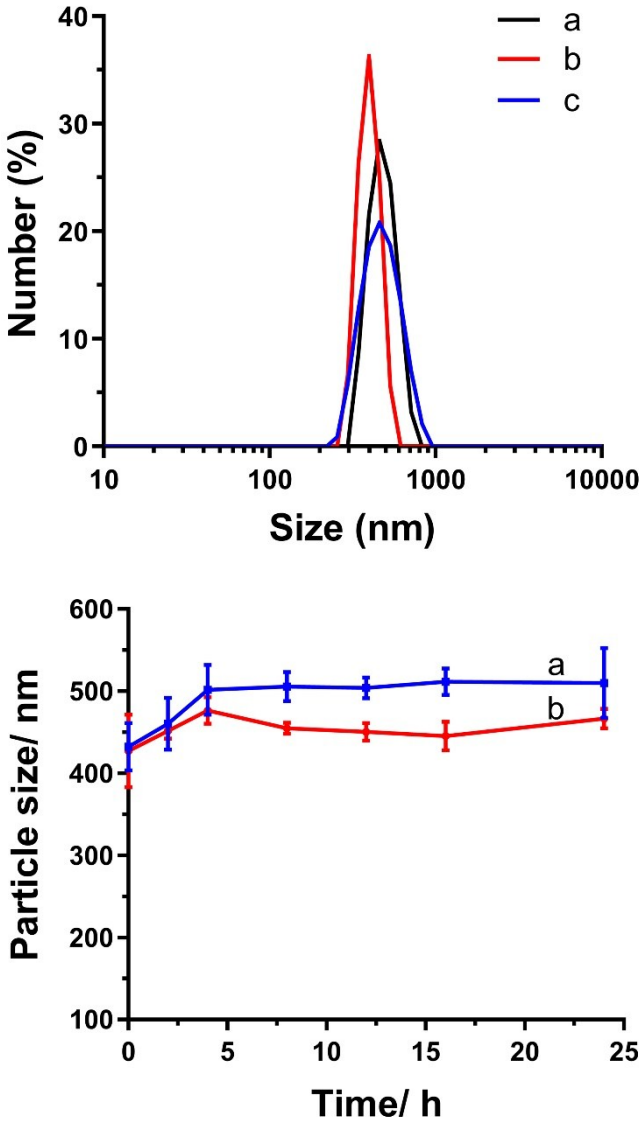

Figure S1. (up) DLS measurement of ***ABC*** type heterotrimeric nanoparticles (a), J-SNPs (b), S-SNPs (c). The three nanoparticles are dispersed in water with a polydispersity index (PDI) less than 0.3. (bottom) DLS profiles of S-SNPs (a) and J-SNPs (b) dispersed in PBS for 24 h.

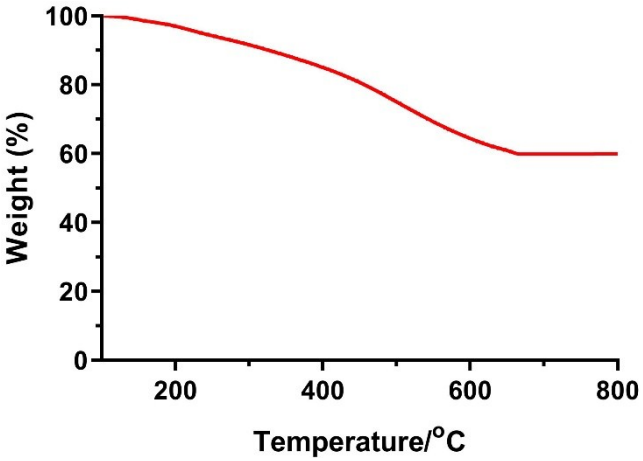

Figure S2. TGA profile of the ***ABC*** type heterotrimeric nanoparticles.

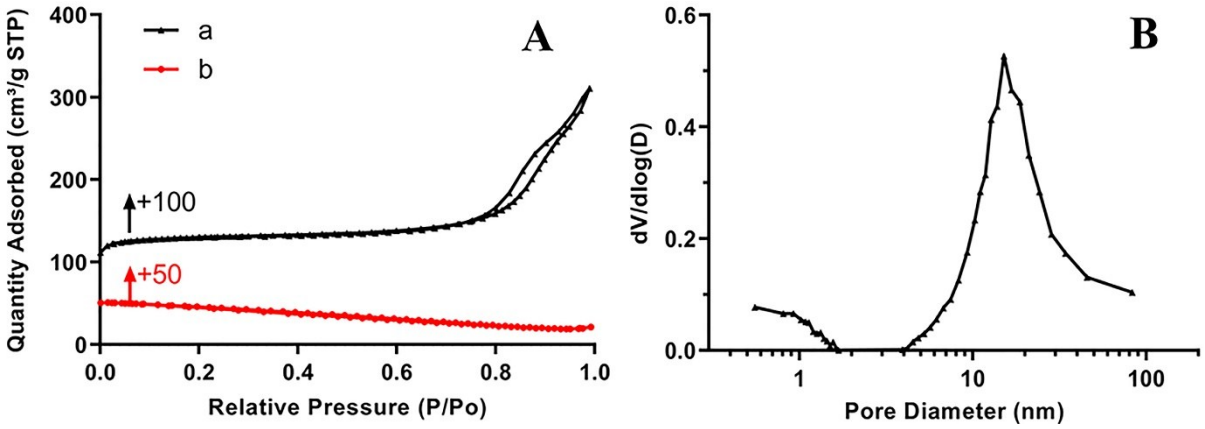

Figure S3. N_2 sorption isotherm (A) and pore size distribution (B) of J-SNPs (a), ***ABC*** type heterotrimeric nanoparticles (b).

Further discussions: N_2 sorption-desorption analysis was conducted to characterize the porous structures (Figure S3). The ***ABC*** type heterotrimeric nanoparticles showed a solid structure. The nitrogen sorption isotherms of J-SNPs were type IV, typical of mesoporous materials. J-SNPs exhibited a pore size of 15.1 nm, a specific surface area of 97.6 $m^2 \cdot g^{-1}$, a pore volume of 0.33 $cm^3 \cdot g^{-1}$ (Table S1).

Table S1 Nitrogen sorption data

Samples	BET surface area ($m^2 \cdot g^{-1}$)	t-Plot micropore area ($m^2 \cdot g^{-1}$)	Pore size (nm)	Pore volume ($cm^3 \cdot g^{-1}$)
ABC type heterotrimeric nanoparticles	2.4	--	--	--
J-SNPs	97.6	59.0	15.1	0.33

***Further discussions on growth models in Figure 3*:** The as-synthesised sample from *A+B* growth model is shown in Figure 3a&e. Particles with two sizes (~300 nm and ~750 nm) were observed. The corresponding calcined sample only showed the existence of the smaller size nanoparticles (~300 nm, Figure 3b). This demonstrated the small and large size nanoparticles should be attributed to silica nanoparticles and APF polymer spheres (removed during calcination), respectively. The above observation confirmed the *A+B* growth model, where *A* refers to silica nanosphere and *B* refers to APF polymer sphere. In the *A@B* growth model, the strong interaction between silica and APF polymer resulted in the formation of spherical APF/silica composite (Figure 3c&e). The fast hydrolysis and condensation rate of TEOS resulted in the formation of silica cores. The copolymerized silica primary particles and APF formed the composite shell coated on the cores. The APF/silica composite can be converted to spherical silica nanoparticles (Figure 3d) where the nano spikes-like silica subunit uniformly coated on the silica core surface, further supported the *A@B* growth model.

Further discussion on time dependent study in Figure 3: To investigate the formation mechanism of the ***ABC*** type heterotrimeric nanoparticles, time-dependent TEM studies were conducted on the intermediate structures collected at various reaction time and their corresponding silica structures (Figure 3). At 5 min since the addition of TEOS, a silica core was formed with a size of ~110 nm. At 10 min, a small nonporous APF polymer "bulge" (block ***B***, low contrast) occurred on one side of the silica core (block ***A***), forming an ***AB*** type heterodimeric Janus structure (Figure 3g). The corresponding calcined sample showed a spherical silica core of ~160 nm (Figure 3g1). The sizes of both blocks ***A*** and ***B*** further increased with time. With the increase of the reaction time to 30 min, a "cap" (block ***C***) was found coated on the other side of the silica core (Figure 3h&h1) and the sizes of "bulge" and "cap" increased with reaction time (Figure 3i&i1), close to the final structure of the ***ABC*** type heterotrimeric nanoparticle.

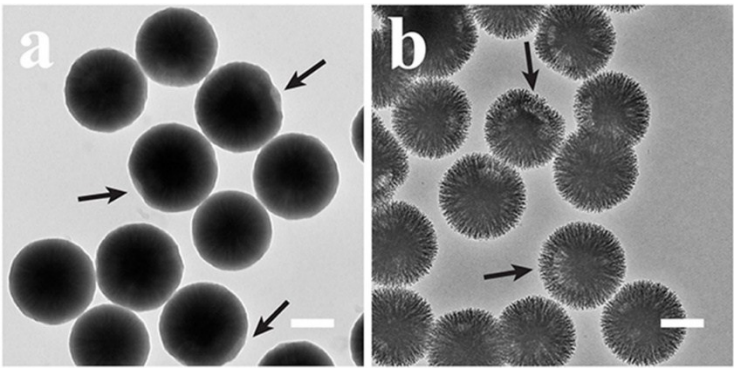

Figure S4. TEM images of APF-silica nanoparticle with 0.20 mL EDA. As synthesized samples (a) and calcined samples (b). All scale bars are 200 nm.

Further discussions: when the EDA amount was increased from 0.175 to 0.20 mL, the size of block ***B*** decreased (Figure S4) because the growth of block ***C*** was accelerated, thus leaving reduced time for block ***B*** growth.

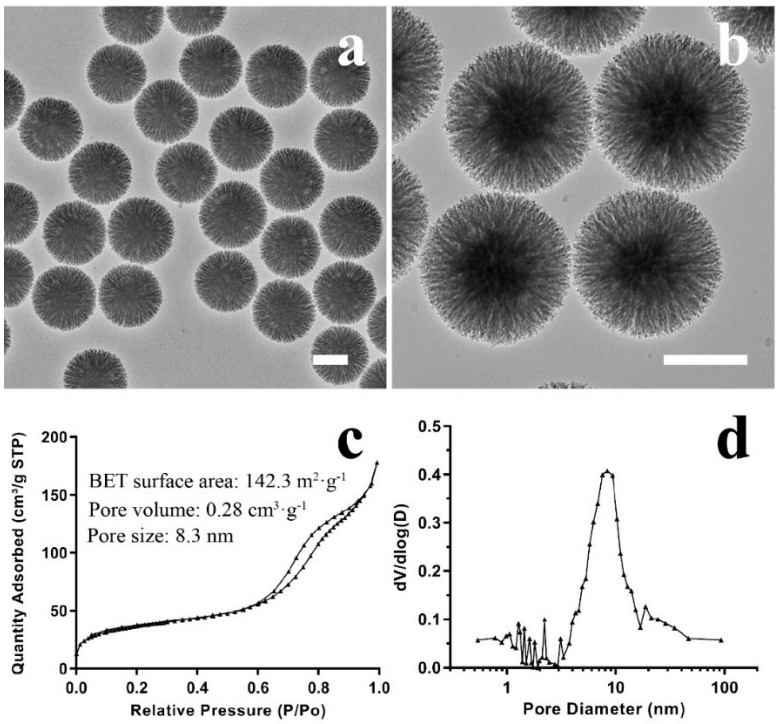

Figure S5. Low (a) and high (b) magnification TEM images; N_2 sorption isotherm (c) and pore size distribution (d) of the S-SNPs obtained by calcination of APF-silica nanocomposite synthesized at an EDA amount of 0.22 mL. All scale bars are 200 nm.

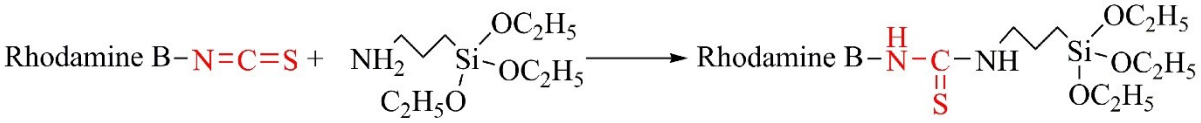

Figure S6. Chemical reaction of RITC with APTES.

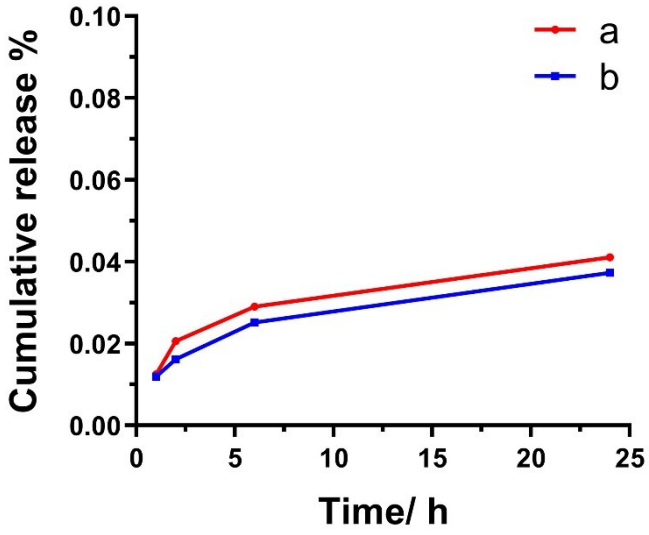

Figure S7. Release profiles of rhodamine-B from J-SNPs (a) and S-SNPs (b).

Further discussions: The RITC was chemically grafted on the silica nanoparticles (Figure S6) and neglectable amount of rhodamine-B was released from the nanoparticles during the cell experiment (Figure S7).

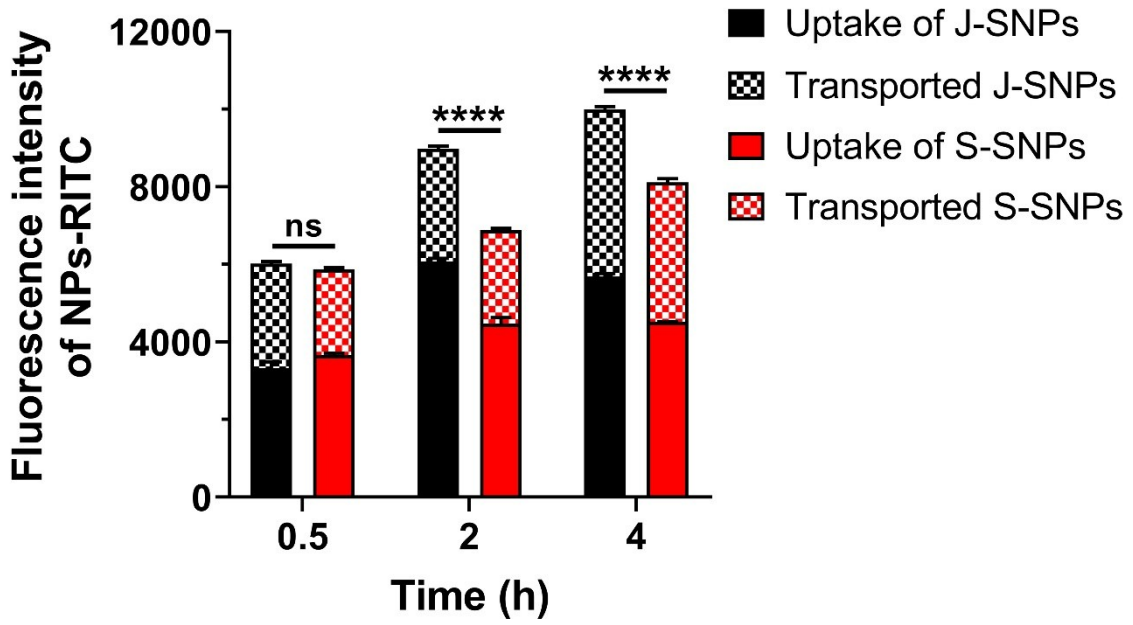

Figure S8. Normalized fluorescence intensity of J-SNPs and S-SNPs (labelled by RITC) transported through or uptake by the in vitro human intestine Caco-2/M-cell monolayer. Statistical analyses were performed by using two-way ANOVA. "ns" indicates not significant ($p>0.05$) and **** indicates significant difference ($p < 0.0001$).

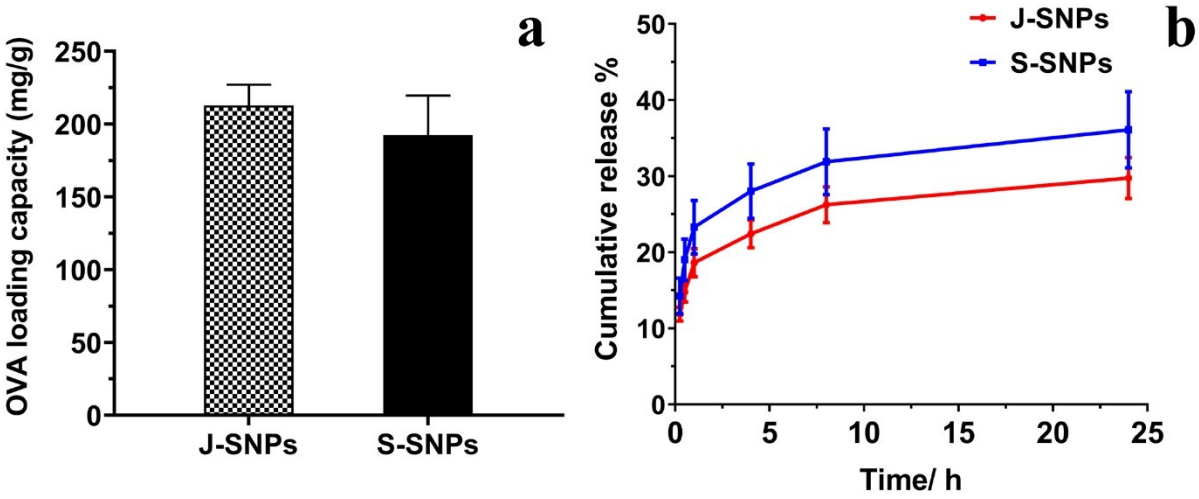

Figure S9. OVA loading capacity of J-SNPs and S-SNPs in PBS (pH 7.4) (a), and cumulative release of OVA from J-SNPs and S-SNPs (b).

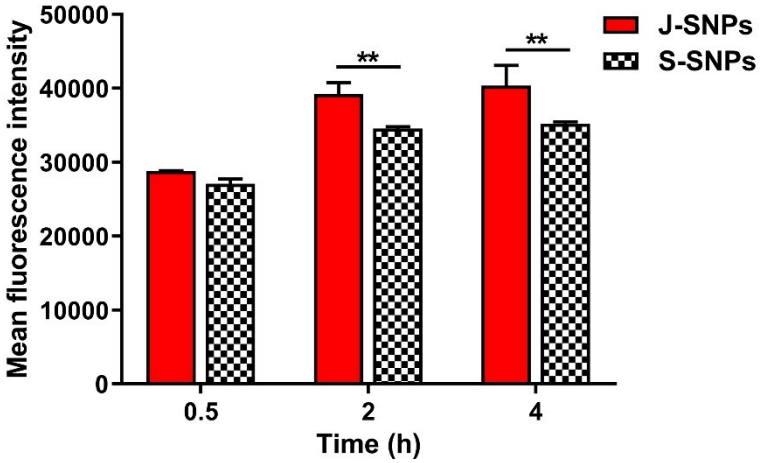

Figure S10. Cellular uptake of FITC-OVA loaded J-SNPs and S-SNPs by the human intestine Caco-2/M-cell monolayer evaluated by FACS. Statistical analyses were performed by using two-way ANOVA. ** $p < 0.01$.

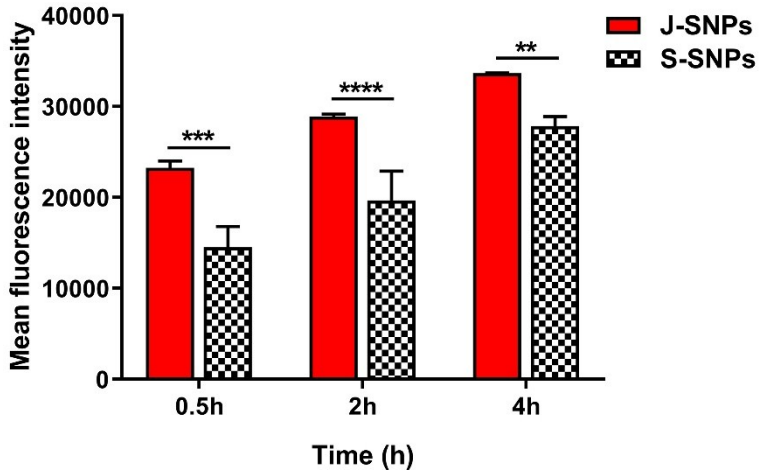

Figure S11. Cellular uptake of FITC-OVA loaded J-SNPs and S-SNPs by Raji B cells evaluated by FACS. Statistical analyses were performed by using two-way ANOVA. ** $p < 0.01$, *** $p < 0.001$, **** $p < 0.0001$.

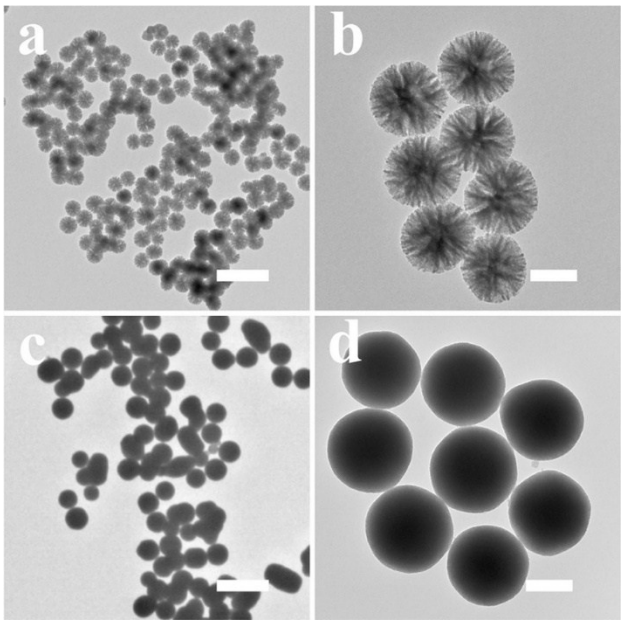

Figure S12. High (a, c) and low (b, d) magnification TEM images of DMSNs (a, b) and MCM-48 (c, d). Scale bars are 1 μm in a, c and 200 nm in b, d.

"***Further discussion*:** High and low magnification TEM images of DMSNs and MCM-48 show that the nanoparticles have comparable size with that of J-SNPs and S-SNPs (Figure S12), which is further supported by DLS measurement (Figure S13). Moreover, N_2 adsorption-desorption analysis results of the DMSNs and MCM-48 are shown in Figure S14, demonstrating the large pore size of DMSNs and the small pore size of MCM-48. OVA loading capacity of DMSNs and MCM-48 in PBS were measured. Results show that MCM-48 and DMSNs have loading capacity of 170 and 270 μg/mg, respectively (Figure S15)."

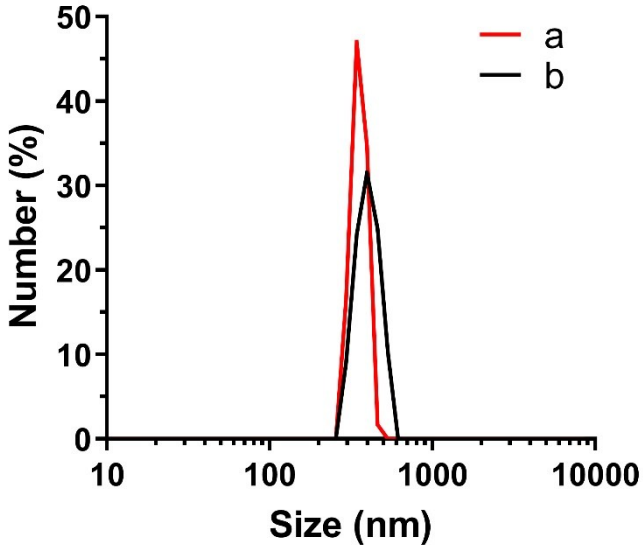

Figure S13. DLS measurement of DMSNs (a), MCM-48 (b).

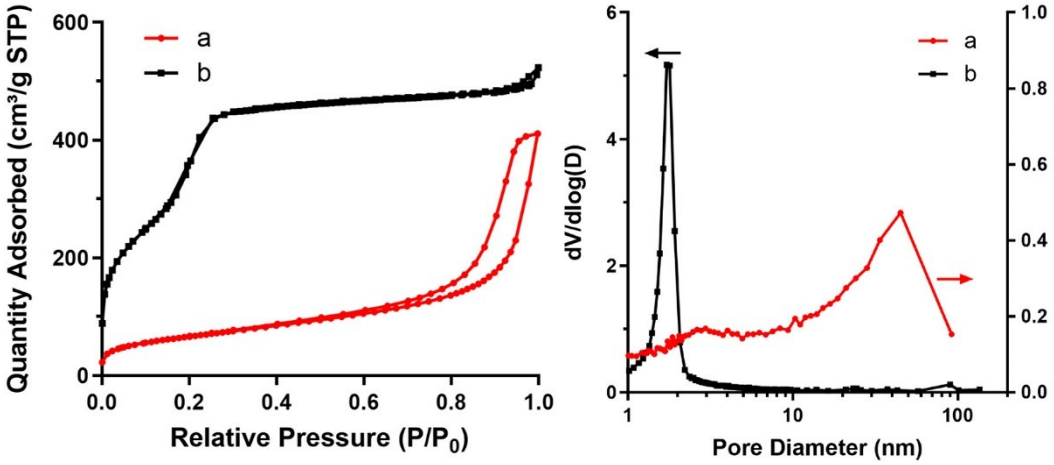

Figure S14. N_2 adsorption-desorption isotherm (left) and pore size distribution curves (right) of DMSNs (a) and MCM-48 (b).

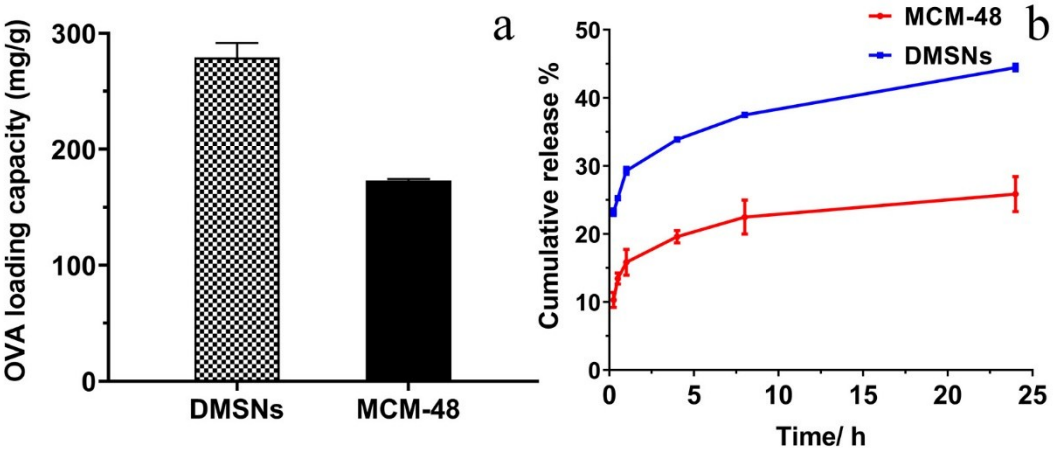

Figure S15. OVA loading capacity of DMSNs and MCM-48 in PBS (a), and cumulative release of OVA from DMSNs and MCM-48 (b).

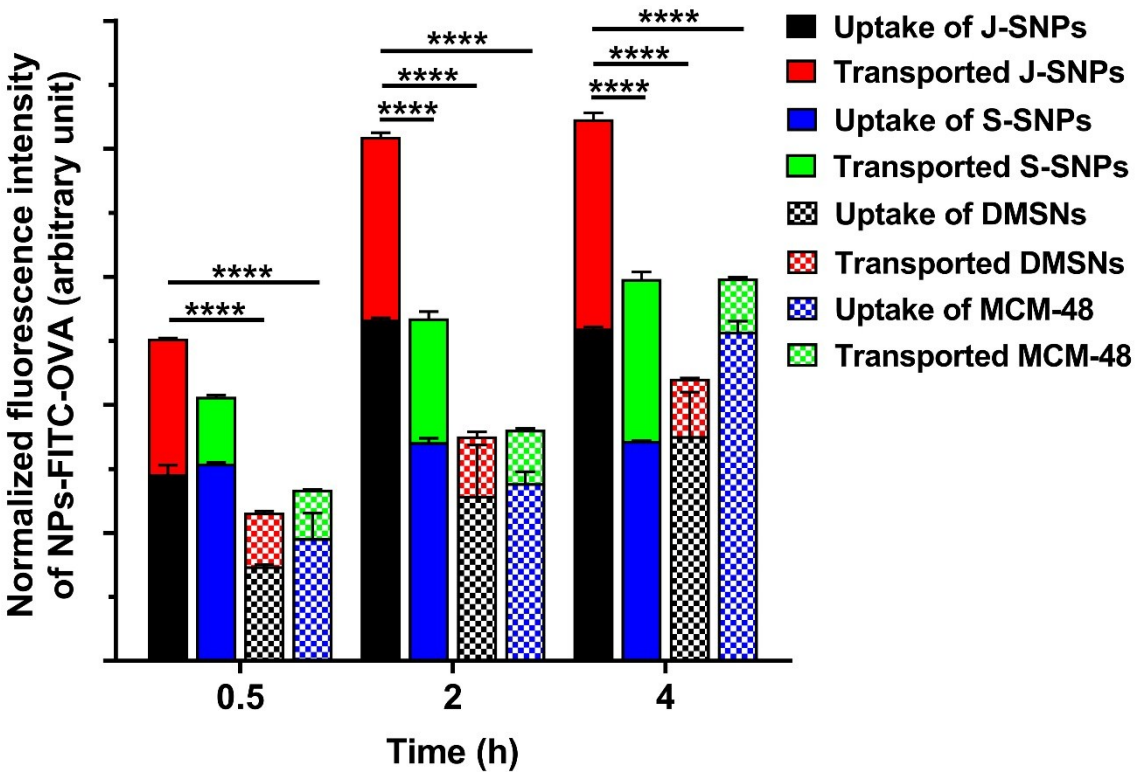

Figure S16. Fluorescence intensity of FITC-OVA loaded J-SNPs, S-SNPs, DMSNs and MCM-48 transported through or uptake by the human intestine mimicking Caco-2/M-cell monolayer model. **** $p < 0.0001$.

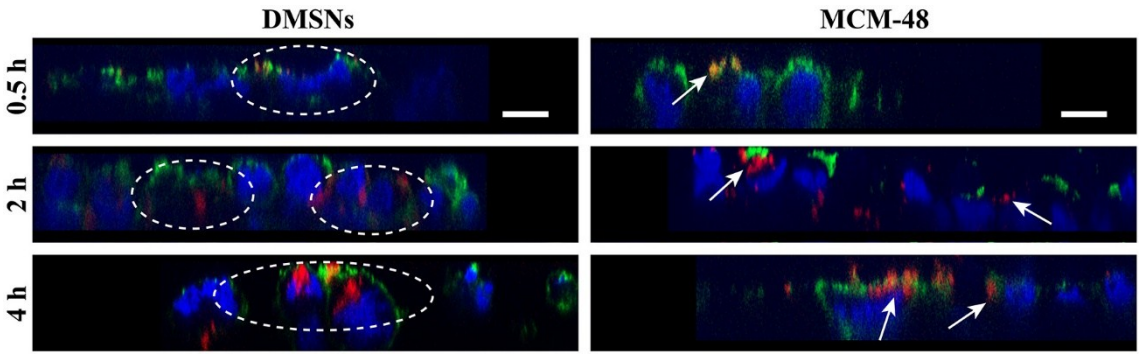

Figure S17. Fluorescence microscopic Z-scans of the Caco-2/M-cell monolayer incubated with DMSNs and MCM-48 (labelled by RITC, red) for 0.5, 2 and 4 h. Cell nuclei were stained with Hoechst (blue). M cell borders were stained with wheat germ agglutinin Alexa Fluor 488 (green) in d. All scale bars are 10 μm.

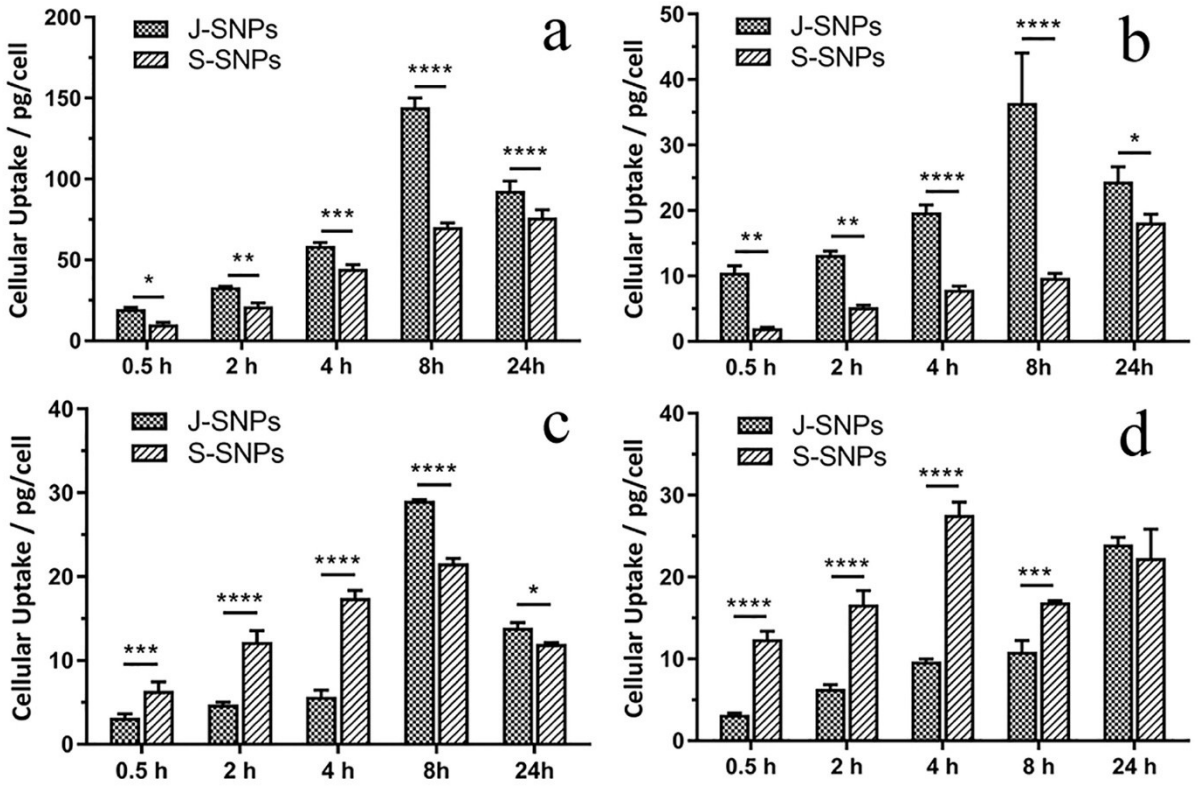

Figure S18. Time dependent cellular uptake of J-SNPs and S-SNPs in four cell lines investigated by ICP-OES. RAW264.7 cells (a); HCT116 cells (b); CHO-K1 cells (c); KHOS cells (d). Statistical analyses were performed by using two-way ANOVA. * indicates $p < 0.05$, ** $p < 0.01$, *** $p < 0.001$, **** $p < 0.0001$.

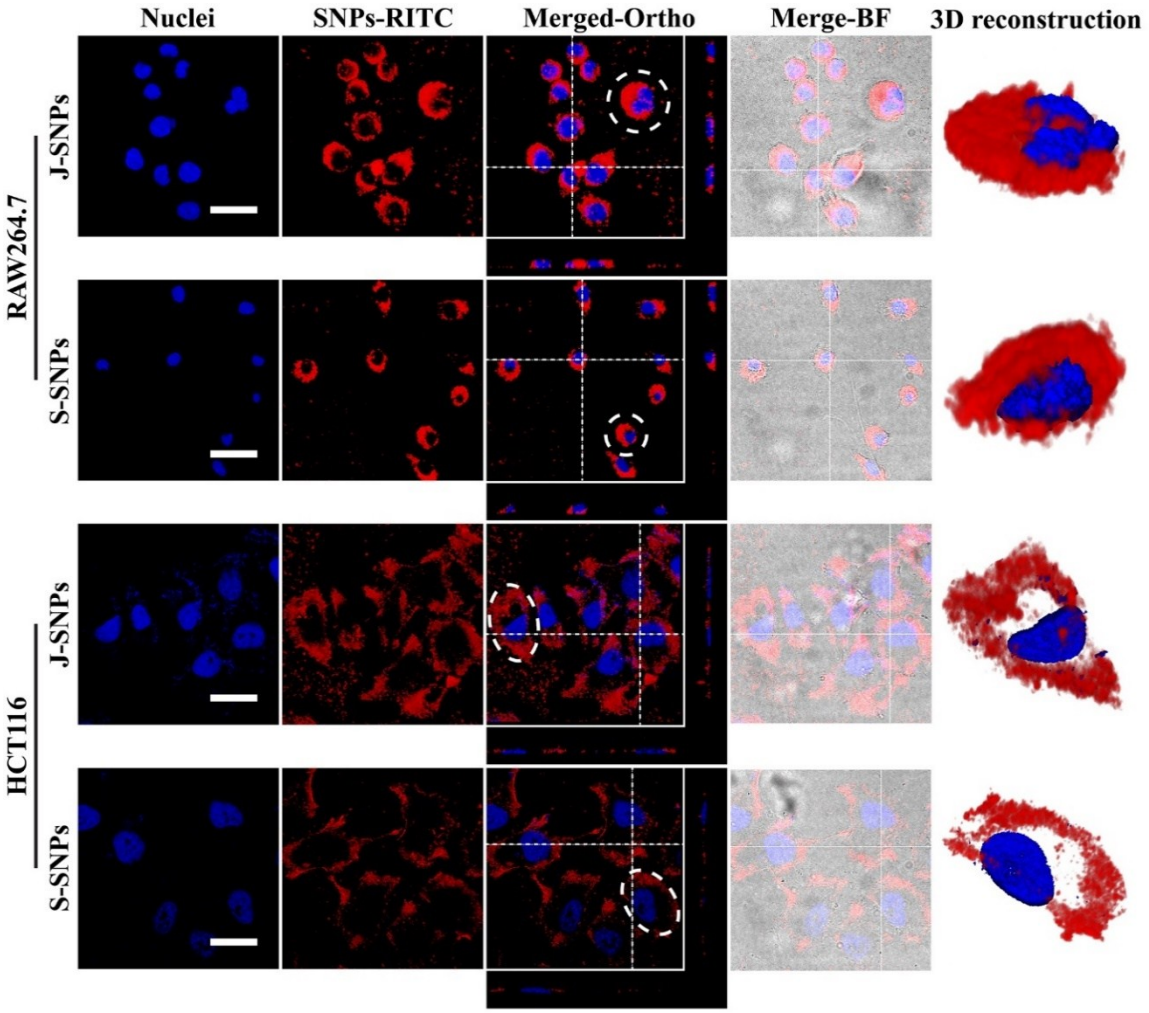

Figure S19. Uptake of fluorescein-labelled J-SNPs or S-SNPs (red) in RAW264.7 and HCT116 cell lines at a nanoparticle concentration of 50 μg/mL. Confocal images of cells incubated with J-SNPs or S-SNPs for 4 h. Orthogonal side-views from z-stack confocal images reveal the presence of J-SNPs or S-SNPs at the cytosol around the nuclei (stained by DAPI, blue). Overlay of bright-field and fluorescence images are noted as Merge-BF. 3D reconstruction of a selected cell (marked by dashed circle) further confirm the uptake of J-SNPs or S-SNPs into the cells. All scale bars are 20 μm.

***Further discussion*:** To demonstrate the uptake of J-SNPs or S-SNPs by cells, confocal fluorescence microscopy study was performed. As shown in Figure S19&S20, the red

fluorescence and the 3D reconstruction images confirmed the presence of J-SNPs or S-SNPs inside the cells.

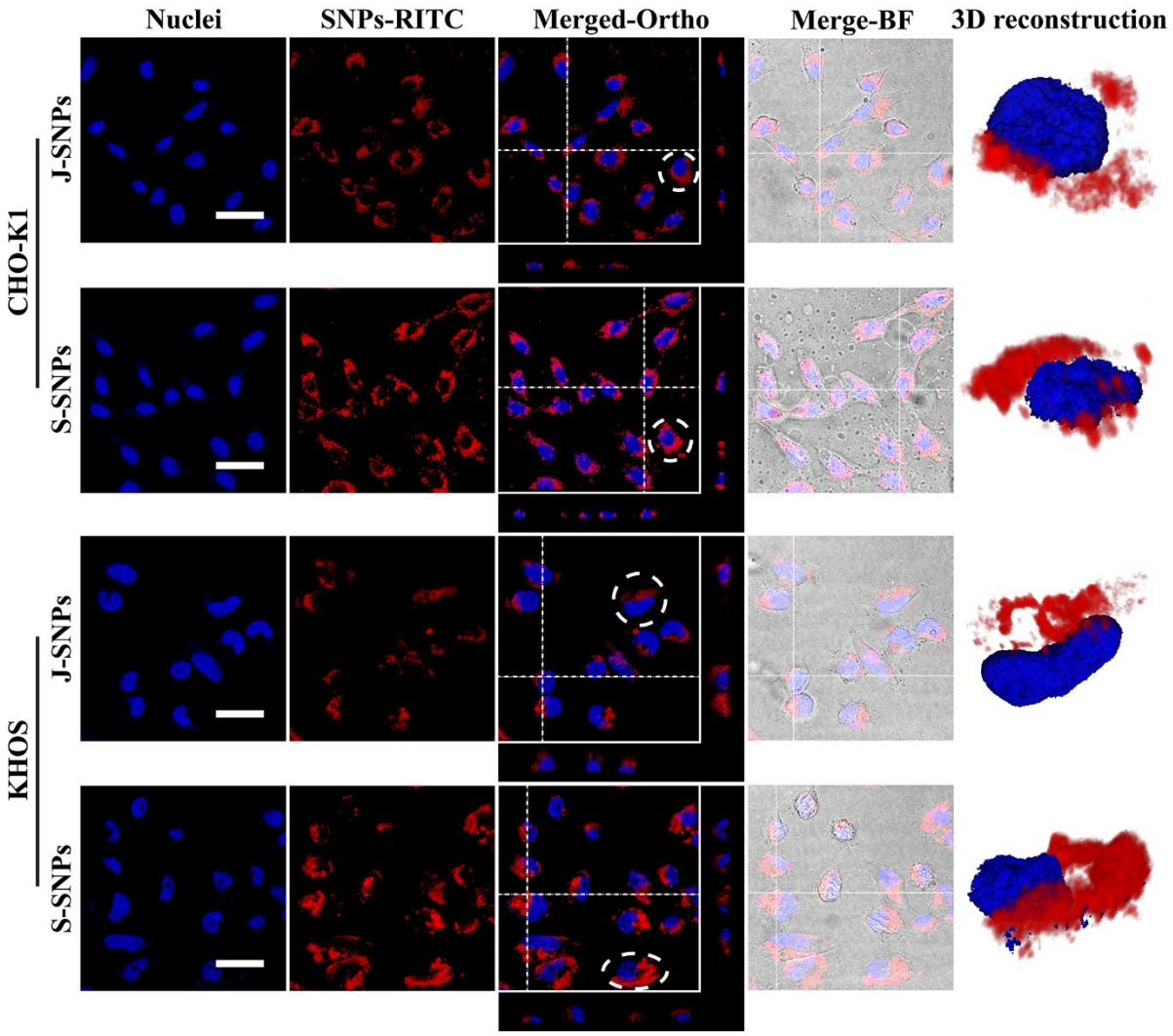

Figure S20. Uptake of fluorescein-labelled J-SNPs or S-SNPs (red) in CHO-K1 and KHOS cell lines at a nanoparticle concentration of 50 μg/mL. Confocal images of cells incubated with J-SNPs or S-SNPs for 4 h. Orthogonal side-views from z-stack confocal images reveal the presence of J-SNPs or S-SNPs at the cytosol around the nuclei (stained by DAPI, blue). Overlay of bright-field and fluorescence images are noted as Merge-BF. 3D reconstruction of a selected cell (marked by dashed circle) further confirm the uptake of J-SNPs or S-SNPs into the cells. All scale bars are 20 μm.

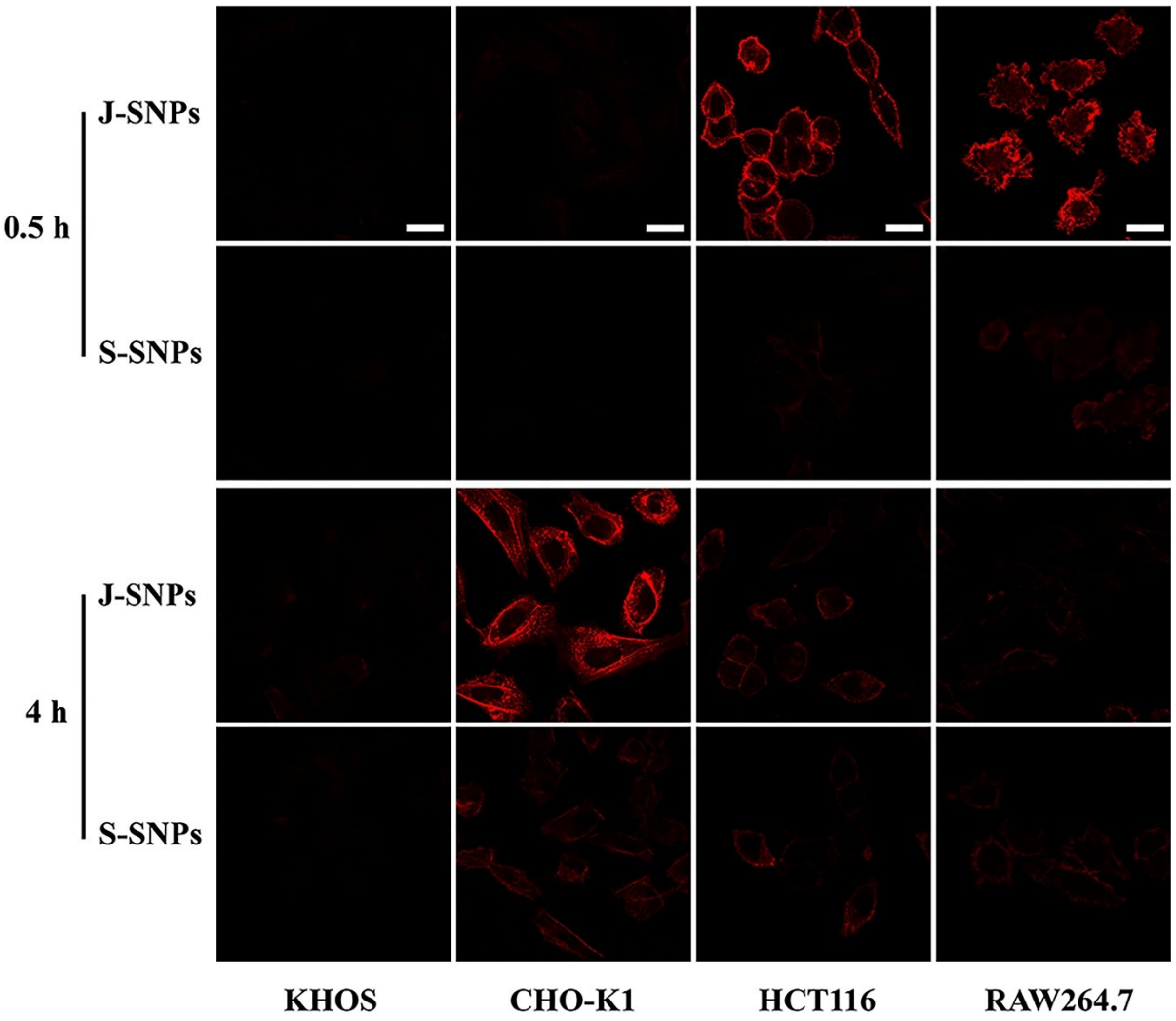

Figure S21. Fluorescent images of KHOS, CHO-K1, HCT116 and RAW264.7 cell lines, after the addition of the J-SNPs and S-SNPs, being fixed at 0.5 or 4 h and stained for polymerized actin with RH phalloidin. All scale bars are 20 μm

***Further discussion*:** To further understand the opposite uptake trend of J-SNPs and S-SNPs in the four cell lines, the activation of the phagocytosis was studied by incubating the J-SNPs and S-SNPs with each cell line at various incubation time (0.5, 2 (Figure S23) and 4 h). It is reported that in cells, an apparent equilibrium exists between actin monomers (G-actin) and actin filaments (F-actin): G-actin is the building block for F-actin and F-actin can depolymerize back to G-actin.[6] When phagocytosis is activated, G-actin polymerizes and forms F-actin. Rhodamine phalloidin (noted as RH phalloidin, red fluorescence) has been widely used to specifically bind and stain F-actin rather than G-actin as an indicator of the activation of

phagocytosis pathway.[7,8] The phagocytosis extent was determined by the intensity of the red fluorescence in each image.[9] As shown in Figure S21-S24, for KHOS cells with negligible phagocytic capability, no significant red fluorescent signal was observed during 4 h incubation with J-SNPs or S-SNPs. For CHO-K1 cells with low phagocytic capability, weak red fluorescence was observed at 2 h (indication of phagocytosis occurred) while strong red fluorescence was observed at 4 h of incubation. The red fluorescence intensity was stronger in J-SNPs treated CHO-K1 cells than that in S-SNPs treated group. For HCT116 and RAW264.7 cell lines, strong red fluorescence was observed in J-SNPs group at 0.5 h, indicating that these two cell lines exhibited fast and intense phagocytosis of J-SNPs at early time point because of their higher phagocytic capability.[10,11] Moreover, the phagocytosis induced by J-SNPs was stronger than that of S-SNPs, similar to CHO-K1 cells. The fast phagocytosis of RAW264.7 and HCT116 cells suggests that under the presence of environment stimuli (J-SNPs or S-SNPs), G-actin in these cells quickly assembled into F-actin, resulting in in-creased content of F-actin. After the burst phagocytosis is completed, F-action can easily dissociate into G-actin,[12] thus the red intensity decreased, consistent with a previous report.[13] From the time when strong red fluorescence occurred and disappeared, the phagocytic capability of the four cell lines is in the order of RAW264.7 > HCT116 > CHO-K1 > KHOS cells. The quantified results (Figure S25) from the related images further confirm the observation.

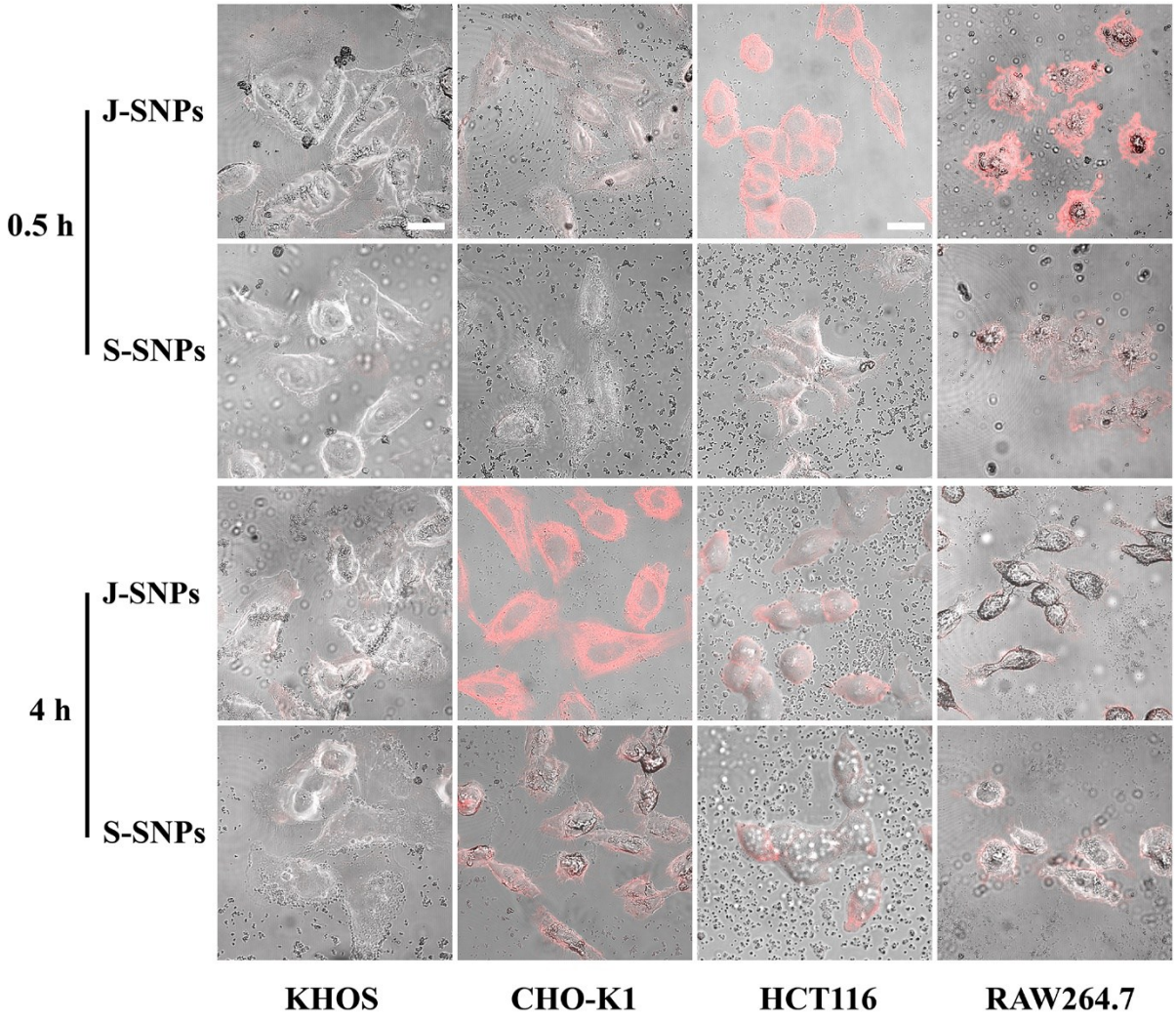

Figure S22. Merged images of KHOS, CHO-K1, HCT116 and RAW264.7 cell lines, after the addition of the J-SNPs and S-SNPs, being fixed at 0.5 or 4 h and stained for polymerized actin with RH phalloidin. All scale bars are 20 μm.

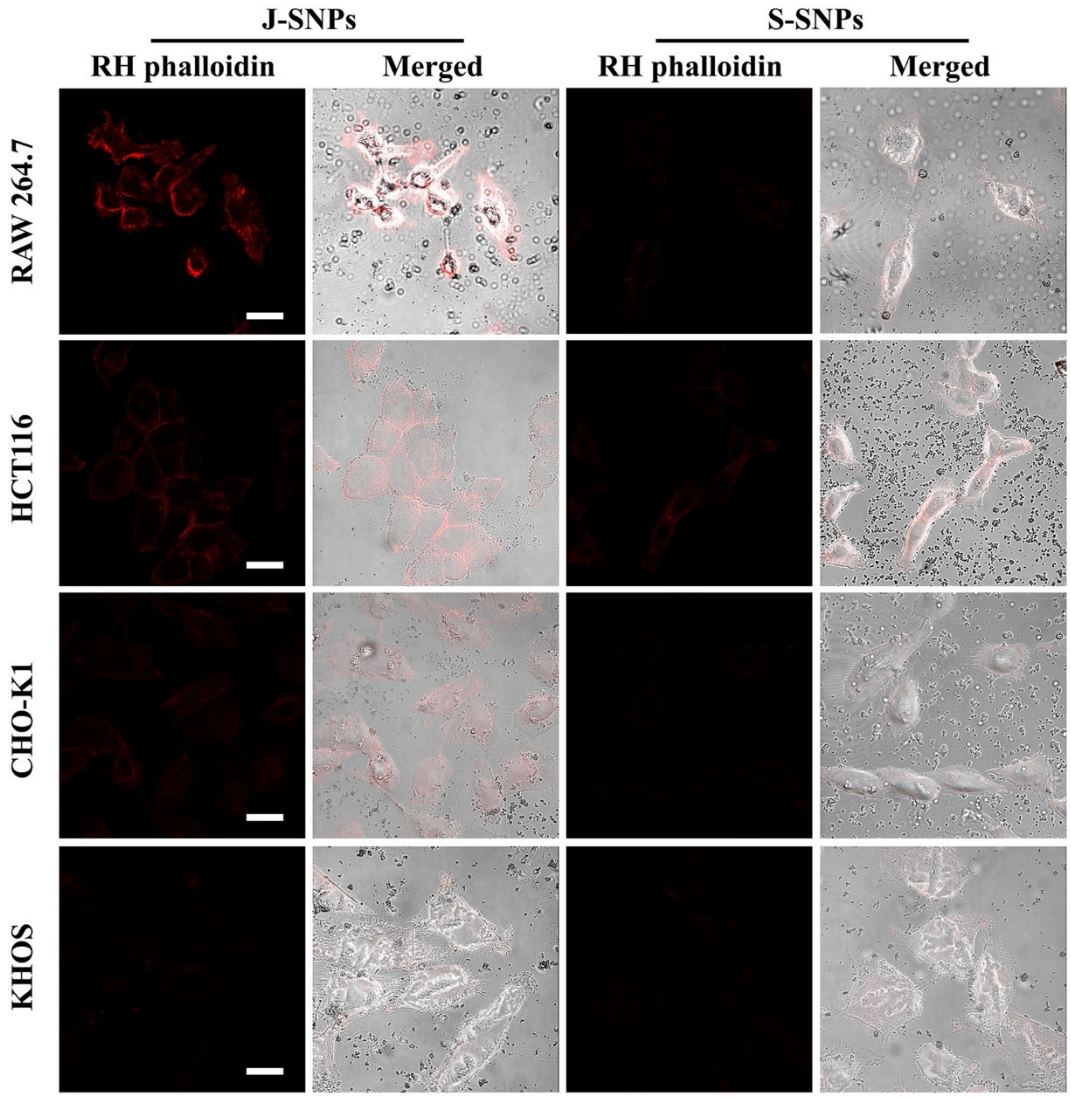

Figure S23. Fluorescent and merged images of four cell lines, after the addition of the J-SNPs and S-SNPs, being fixed at 2 h and stained for polymerized actin with RH phalloidin. All scale bars are 20 μm.

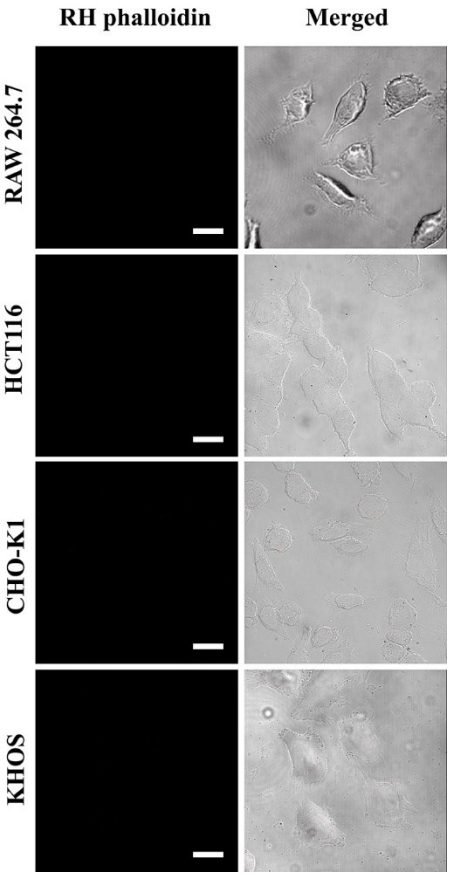

Figure S24. Fluorescent and merged images of four cell lines stained by RH phalloidin without the addition of silica nanoparticle (control group). All scale bars are 20 μm.

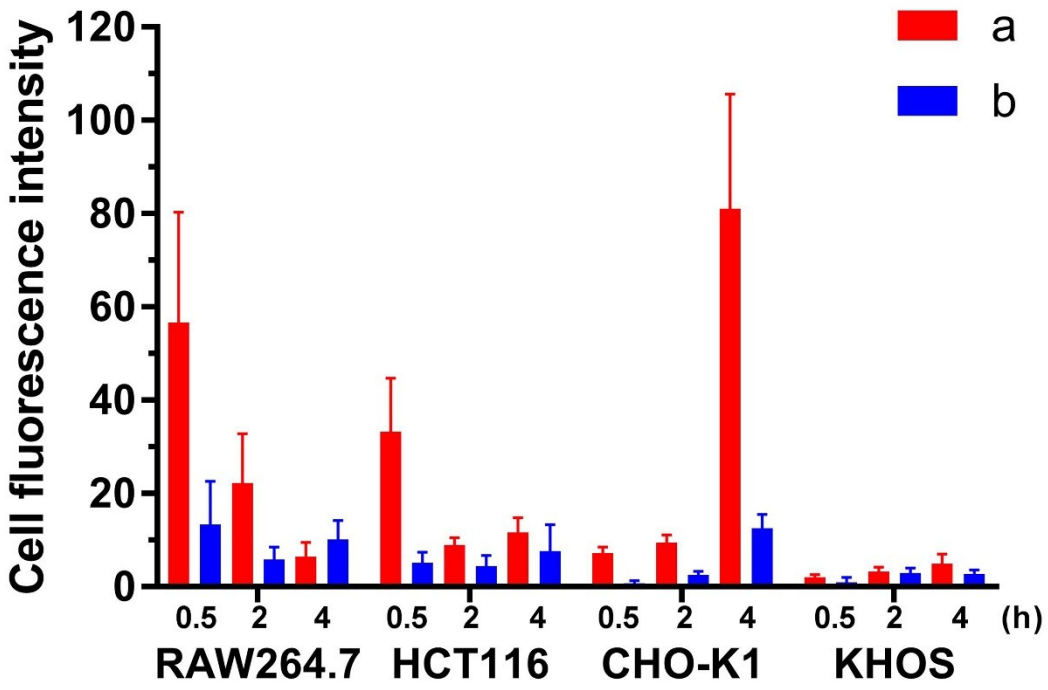

Figure S25. The red fluorescence intensity calculated from Figure S22&S23 by software (Image J). Cells incubated with J-SNPs (a) and S-SNPs (b) at different incubation time (0.5, 2 and 4 h). J-SNPs can stimulate actin polymerization and exhibited stronger red fluorescence signal compared to S-SNPs in RAW264.7 (0.5 h), HCT116 (0.5 h) and CHO-K1 (4 h) cell lines.

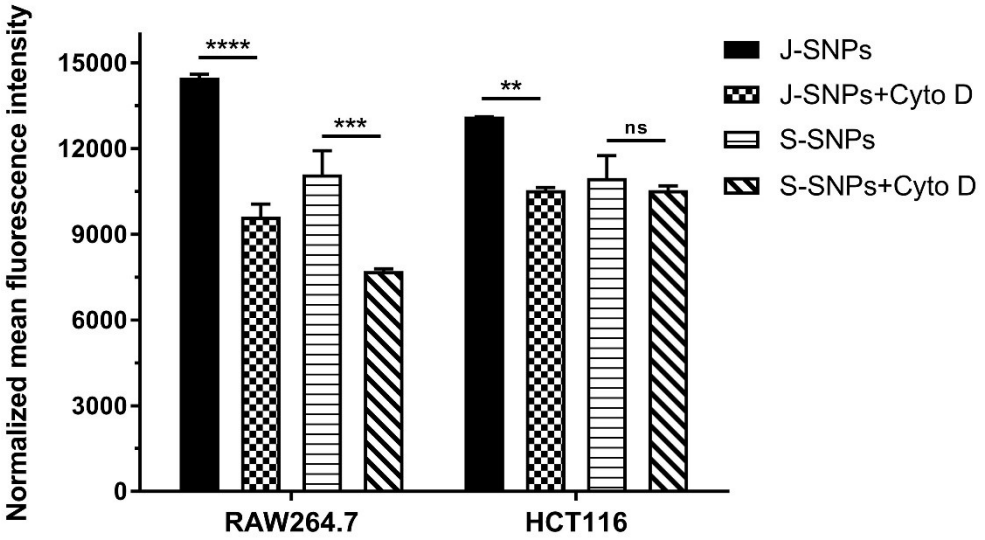

Figure S26. The effects of phagocytosis inhibitor Cyto D on the cellular uptake of the J-SNPs and S-SNPs in RAW264.7 and HCT116 cell lines evaluated by FACS. Statistical analyses were performed by using two-way ANOVA. * indicates $p < 0.05$, ** $p < 0.01$, *** $p < 0.001$, **** $p < 0.0001$.

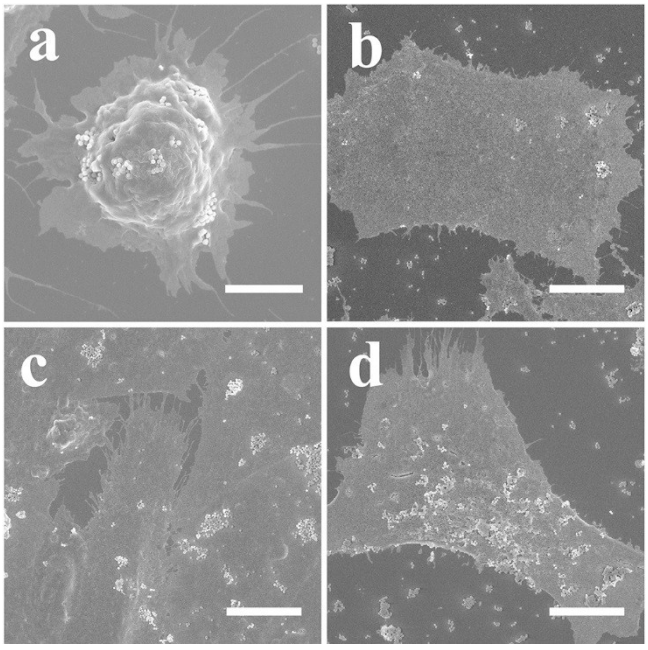

Figure S27. Low magnification SEM images of the four cells lines incubated with J-SNPs for 1 h, RAW264.7 (a), HCT116 (b), CHO-K1 (c), and KHOS (d). Scale bars, 5 μm (a) and 10 μm (b, c, d).

Further discussion: From Figure S27, the low magnification SEM images showed that RAW264.7 cells exhibited a round morphology, while HCT116, CHO-K1, and KHOS cells exhibited a more spread and elongated flattened structure. Cell filopodia can be clearly observed. J-SNPs (smaller contrast) were observed attaching on the cell membrane.

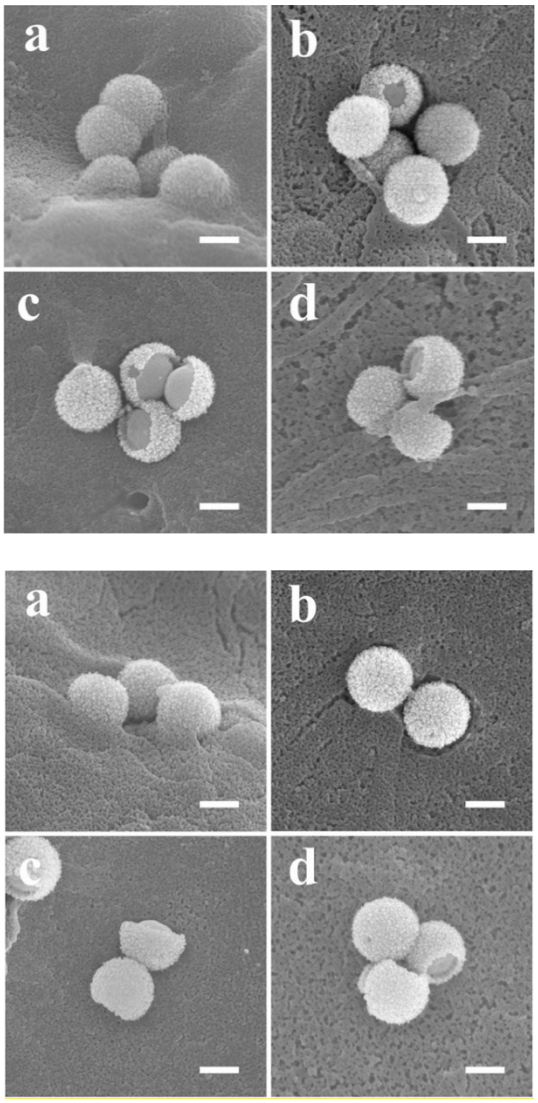

Figure S28. Two sets of representative SEM images of the four cells lines incubated with J-SNPs for 1 h, RAW264.7 (a), HCT116 (b), CHO-K1 (c), and KHOS (d). Cells were fixed with formaldehyde and osmium tetroxide, which were subsequently coated in gold. All scale bars are 200 nm.

Further discussion: It has been reported that the initiation of phagocytosis is determined by the local shape of the particles when contacting with cell membrane, whereas the contact angle plays a key role.[14] For example, rod-like particles can easily initiate phagocytosis at the tip side.[15] Oblate ellipsoids are also more efficiently internalized by macrophages than spherical ones.[16] In our case, compared to S-SNPs, the unique "dent" part of the J-SNPs is similar to an

"oblate" structure, which can increase the possibility of nanoparticle interacting with the cell membrane and favour phagocytosis.[14]

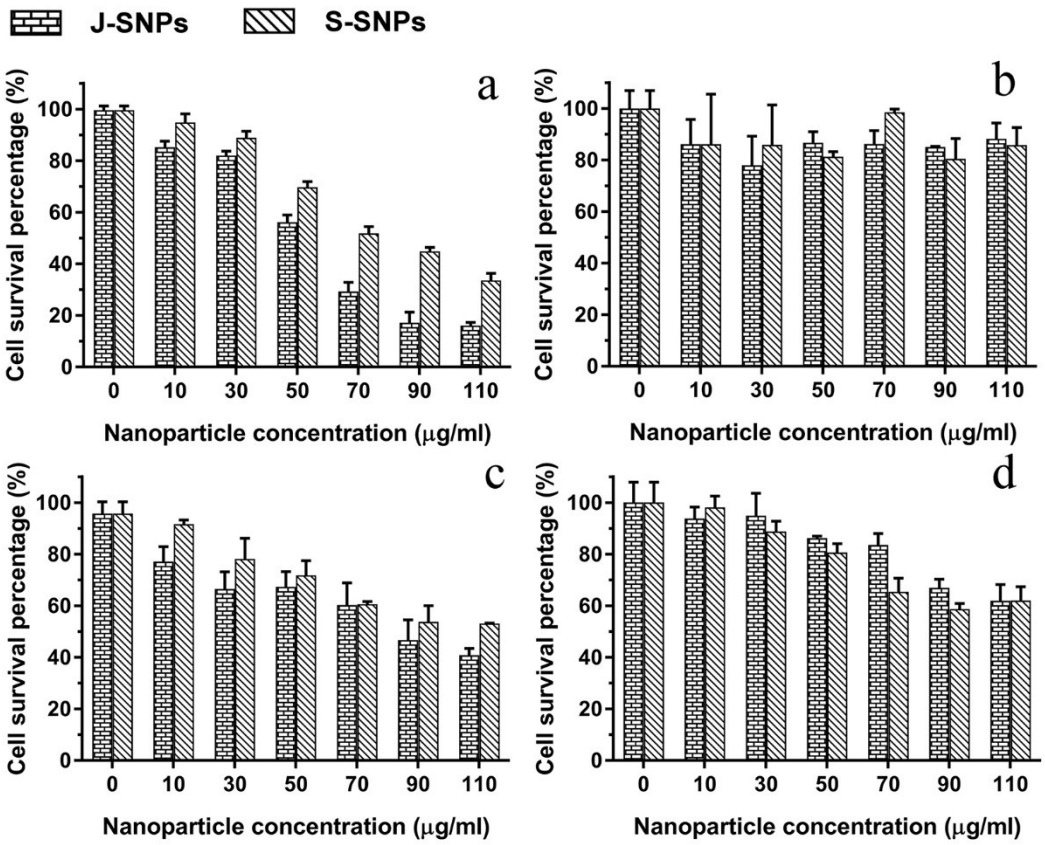

Figure S29. Cytotoxicity evaluated by MTT assay in the range of 0-110 μg/mL of J-SNPs or S-SNPs incubated with cells for 24 h. RAW264.7 (a), HCT116 (b), CHO-K1 (c) and KHOS cell lines.

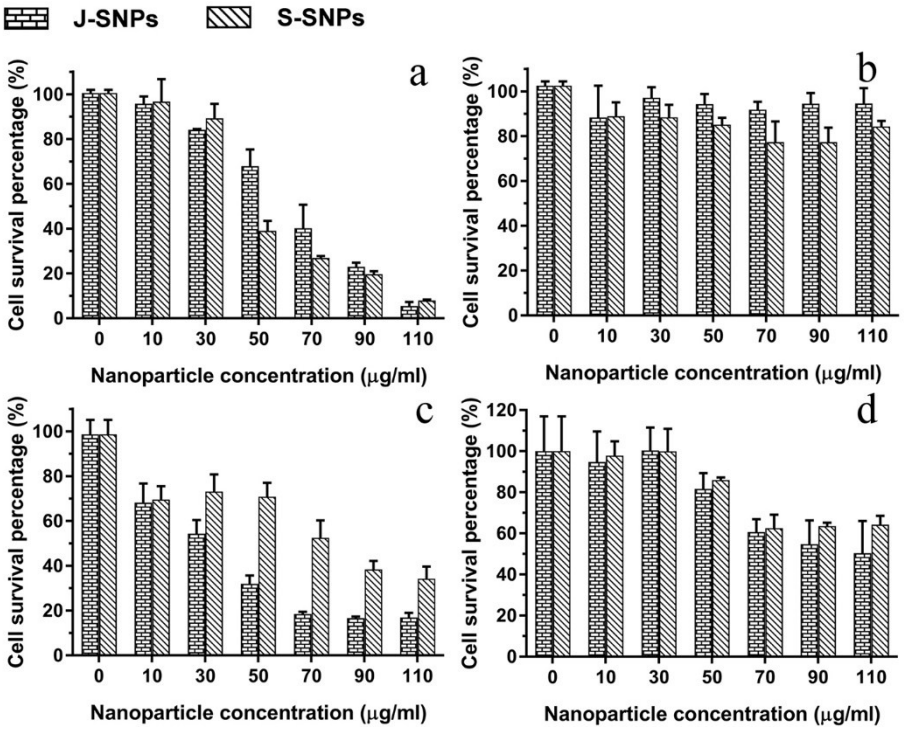

Figure S30. Cytotoxicity evaluated by MTT assay in the range of 0-110 μg/mL of J-SNPs or S-SNPs incubated with cells for 72 h. RAW264.7 (a), HCT116 (b), CHO-K1 (c) and KHOS cell lines.

References

(1) T. W. Kim, P. W. Chung, V. S. Y. Lin, Facile synthesis of monodisperse spherical MCM-48 mesoporous silica nanoparticles with controlled particle size. *Chem. Mater.* 2010. **22**, 5093.

(2) Y. Yang, S. Bernardi, H. Song, J. Zhang, M. Yu, J. C. Reid, E. Strounina, D. J. Searles, C. Yu, Anion assisted synthesis of large pore hollow dendritic mesoporous organosilica nanoparticles: understanding the composition gradient. *Chem. Mater*. 2016. **28**, 704.

(3) M. J. Uddin, H. S. Gill, Ragweed pollen as an oral vaccine delivery system: Mechanistic insights. *J. Control. Release* 2017, **268**, 416.

(4) A. des Rieux, V. Fievez, I. Théate, J. Mast, V. Préat, Y. J. Schneider, An improved in vitro model of human intestinal follicle-associated epithelium to study nanoparticle transport by M cells. *Eur. J. Pharm. Sci*. 2007, **30**, 380.

(5) C. Schimpel, B. Teubl, M. Absenger, C. Meindl, E. Fröhlich, G. Leitinger, A. Zimmer, E. Roblegg, Development of an advanced intestinal in vitro triple culture permeability model to study transport of nanoparticles. *Mol. Pharm*. 2014, **11**, 808.

(6) G. M. Cooper, R. E. Hausman, The cell: Molecular approach. Medicinska naklada, 2004.

(7) F. Gittes, B. Mickey, J. Nettleton, J. Howard, Flexural rigidity of microtubules and actin filaments measured from thermal fluctuations in shape. *J. Cell Biol*. 1993, **120**, 923.

(8) M. D. Welch, R. D. Mullins, Cellular control of actin nucleation. *Annu. Rev. Cell Dev. Biol*. 2002, **18**, 247.

(9) F. Castellano, P. Chavrier, E. Caron, Actin dynamics during phagocytosis. *Semin. Immunol*. 2001, **13**, 147.

(10) A. Aderem, D. M. Underhill, Mechanisms of phagocytosis in macrophages. *Annu. Rev. Immunol*. 1999, **17**, 593.

(11) Gagnon, E.; Duclos, S.; Rondeau, C.; Chevet, E.; Cameron, P. H.; Steele-Mortimer, O.; Paiement, J.; Bergeron, J. J.; Desjardins, M. Endoplasmic reticulum-mediated phagocytosis is a mechanism of entry into macrophages. *Cell* 2002, **110**, 119.

(12) M. Diakonova, G. Bokoch, J. A. Swanson, Dynamics of cytoskeletal proteins during Fcγ receptor-mediated phagocytosis in macrophages. *Mol. Biol. Cell* 2002, **13**, 402.

(13) C. C. Scott, W. Dobson, R. J. Botelho, N. Coady-Osberg, P. Chavrier, D. A. Knecht, C. Heath, P. Stahl, S. Grinstein, Phosphatidylinositol-4, 5-bisphosphate hydrolysis directs actin remodeling during phagocytosis. *J. Cell Biol*. 2005, **169**, 139.

(14) J. A. Champion, S. Mitragotri, Role of target geometry in phagocytosis. *Proc. Natl. Acad. Sci. U. S. A*. 2006, **103**, 4930.

(15) J. Möller, T. Luehmann, H. Hall, V. Vogel, The race to the pole: how high-aspect ratio shape and heterogeneous environments limit phagocytosis of filamentous Escherichia coli bacteria by macrophages. *Nano Lett*. 2012, **12**, 2901.

(16) G. Sharma, D. T. Valenta, Y. Altman, S. Harvey, H. Xie, S. Mitragotri, J. W. Smith, Polymer particle shape independently influences binding and internalization by macrophages. *J. Control. Release* 2010, **147**, 408.